POAC'17
Busan, KOREA

Proceedings of the 24th International Conference on
Port and Ocean Engineering under Arctic Conditions
June 11-16, 2017, Busan, Korea

Modelling the Dynamics of Iceberg-Soil Interaction during Seabed Gouging

Jeroen S. Hoving[1], Rutger Marquart[1], Federico Pisanò[2]
[1]Delft University of Technology, Section of Offshore Engineering, Delft, the Netherlands
[2]Delft University of Technology, Section of Geo-Engineering, Delft, the Netherlands

ABSTRACT

Not only in the Arctic, but also well outside the Arctic, icebergs can be a danger to buried offshore pipelines due to seabed gouging. As it is not economically feasible to bury these pipelines at depths where soil deformations are small, these pipelines are buried at sub-gouge depths where the soil experiences significant plastic deformations. Before considering the sub-gouge soil deformations that are vital to determine optimal pipeline burial depths, a better understanding of dynamic iceberg-soil interaction during seabed gouging is required.

In the past, several models have been developed to describe the interaction forces between an iceberg and the soil in front of the iceberg keel based on static soil failure theory or from experimental observations. These models do not fully account for the dynamic behaviour of the iceberg, nor do they consider the corresponding response of the sub-gouge soil. In fact, how the extent of sub-gouge deformations depends on the geotechnical parameters of the seabed is not at all well understood. Therefore, a three-dimensional physics-based model is being developed that describes the transient iceberg-soil interaction (i) based on plasticity theory, (ii) accounting for the dynamic response of the iceberg during gouging and (iii) including the hydrodynamics of the iceberg. This paper presents a two-dimensional version of the iceberg-soil interaction model assuming the iceberg keel to be rigid and plane-strain conditions for the soil. Model predictions are presented and compared for different seabed characteristics.

KEY WORDS: Iceberg dynamics; iceberg-soil interaction; sub-gouge deformation.

INTRODUCTION

Especially in the Arctic and other ice-infested areas, it is attractive to transport hydrocarbons, for example from offshore production locations to shore, or across water bodies between land masses, by means of marine pipelines, thereby largely evading the interaction with sea ice. Nevertheless, icebergs and large ice ridges can be a severe danger to marine pipelines as they ground and gouge the seabed. Generally, marine pipelines in iceberg areas are buried in a trench to protect these pipelines from damage due to iceberg gouging. Figure 1 shows a simplified representation of the interaction between an iceberg keel and the seabed near a pipeline taken from Barrette (2011), where BD is the pipeline burial depth. As Barrette (2011) states, it is not economically feasible to bury pipelines in zone 3, where the soil deformations are negligible and therefore pipelines are buried in zone 2, where the soil experiences significant plastic deformations. Understanding the severity of these sub-gouge deformations is vital

for pipeline design and in particular to determine the required depth of pipeline trenches.

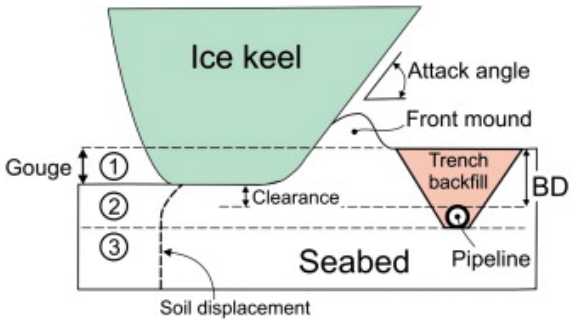

Figure 1. Iceberg keel-seabed interaction near a trenched pipeline (Barrette, 2011).

In the past, several models were developed to describe the interaction between an iceberg keel and the seabed based on static soil failure or from experimental observations. In the two-dimensional gouging models by Kioka and Saeki (1995) and Yoon et al. (1997) for example, assumptions are made that limit the results. The model presented by Kioka and Saeki (1995) assumes that during gouging the iceberg moves with a constant velocity and that the iceberg moves along a so-called pre-described gouging curve, while the gouging model by Yoon et al. (1997) neglects the rotational motion of the iceberg. Clearly, the velocity of an iceberg during gouging is not constant, but decreases due to the soil resistance. In the iceberg-soil interaction model presented in this contribution, the deceleration of the iceberg as it hits and fails the seabed, as well as the rotation of the iceberg, are included to properly account for the dynamic response of the iceberg during seabed gouging. The seabed resistance forces are incorporated into the model quasi-statically, by means of the passive soil-resistance calculated using a slightly adapted version of the theory of Hettiaratchi and Reece (1974).

A PHYSICS-BASED MODEL FOR DYNAMIC ICEBERG-SOIL INTERACTION

Ultimately, it is our aim to develop a three-dimensional physics-based model that describes the transient iceberg-soil interaction that accounts for the plastic deformation of the soil to correctly describe the corresponding soil resistance against iceberg gouging. This paper presents the first stage of this project and regards the two-dimensional version of the iceberg-soil interaction model. The two-dimensional model for dynamic iceberg-soil interaction during seabed gouging is presented here for two separate cases: 1) the free-floating iceberg before grounding, which is aimed at specifically considering the hydrodynamics of the iceberg, and 2) the interaction of the iceberg with the soil as it grounds, specifically focused on the iceberg-soil interaction. In the following, first the general assumptions and modelling constraints, i.e. the assumptions and constraints that apply to both cases, are discussed. Subsequently, the modelling of the two separate cases is discussed and the corresponding model results are presented consecutively. Finally, conclusions regarding the current version of the iceberg gouging model are given and our ideas for future improvements are discussed.

Reference iceberg “Bertha” and the iceberg model

The iceberg-soil interaction model discussed here allows for various iceberg geometries. As a basis for possible iceberg geometries, data is used from the Dynamics of Iceberg Grounding and Scouring (DIGS) field experiments performed in the Eastern Canadian Continental Shelf,

Labrador, in August 1985 (Hodgson et al., 1988). For the purpose of this paper however, from the DIGS experiments, only the iceberg Bertha is considered.

Iceberg Bertha grounded at a water-depth of 107 m on the north-western edge of Makkovik Bank, where water depths range from a minimum of 102 m near the south-eastern end to a maximum of 135 m at the north-western end. At this location, the seabed is relatively smooth and flat with local slopes averaging 1:50. Figure 2a depicts the above- and below-water shape and dimensions of iceberg Bertha that were determined after the iceberg floated free due to a calving event, which additionally caused the iceberg to significantly roll and yaw.

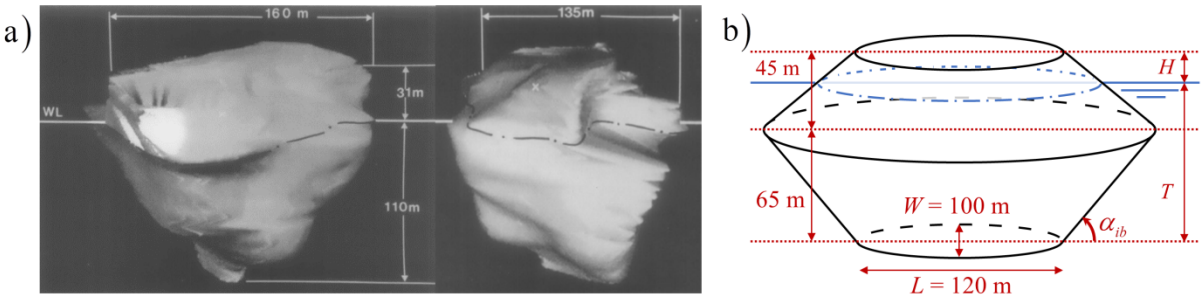

Figure 2. a) Generated perspective of iceberg Bertha (ref Hodgson 1988);
b) Dimensions of iceberg Bertha simplified by two elliptical cone frustums.

The iceberg itself is assumed to be rigid. This means that the iceberg does not deform upon interaction with the water or the soil, nor does it change its shape over time due to thawing or other external influences. To straightforwardly determine the wind and current loads on the iceberg, as well as to calculate the weight and buoyancy of the iceberg, the shape of iceberg Bertha is assumed as depicted in Figure 2b. Maintaining the dimensions of the generated perspective of iceberg Bertha in Figure 2, the ratio between freeboard and keel height, as well as the total volume of the iceberg are too high. The width and length of the elliptical base are therefore respectively chosen as 100 m and 120 m, while the mass and the mass moment of inertia, as well as the freeboard and the keel height of the iceberg model vary depending on the angle α_{ib}. Choosing $\alpha_{ib} = 50°$, the iceberg has a freeboard (H) and a keel height (T) of respectively 18,2 m and 91,8 m, a mass of 2,2 Mt and a mass moment of inertia of 7,0 Gt·m^2.

THE FREE-FLOATING ICEBERG BEFORE GROUNDING

To capture the behaviour of the iceberg during seabed gouging, first it is important to describe the motions of the iceberg before grounding. As long as the iceberg does not interact with the seabed, the iceberg is modelled as a free-floating body, only interacting with the air and the water. This also means that the interaction of the iceberg with other occurrences of ice, such as sea ice or other icebergs, is disregarded.

Figure 3 illustrates the dimensions and the degrees of freedom of the free-floating iceberg, the gravity and buoyancy forces, as well as the aero- and hydrodynamic forces acting on the iceberg. The degrees of freedom of the iceberg, i.e. its surge, heave and pitch, are respectively denoted as x_{ib}, z_{ib} and θ_{ib}. Here, the aero- and hydrodynamic forces applied to the iceberg are all assumed to work in the direction of the x-axis, thus being the direction of forward motion for the iceberg. Additionally, the heave of the iceberg is described in the direction of the z-axis, while θ denotes the pitch of the iceberg.

For large icebergs, the drift of icebergs is governed by ocean currents as the influence of waves on icebergs decreases as the iceberg size increases (Diemand, 2001). Therefore, the contributions of incident, diffracted and radiated waves are assumed negligible, thereby implying that the damping associated with body-induced wave radiation is negligible as well. As a result, only viscous damping is accounted for. Then, as the Coriolis force is a three-dimensional phenomenon and the modelling applied here is two-dimensional, its influence is not included. Additionally, at the scale of an iceberg gouging event, the influence of the Coriolis force is likely to be negligible and iceberg trajectories may be assumed as a straight line.

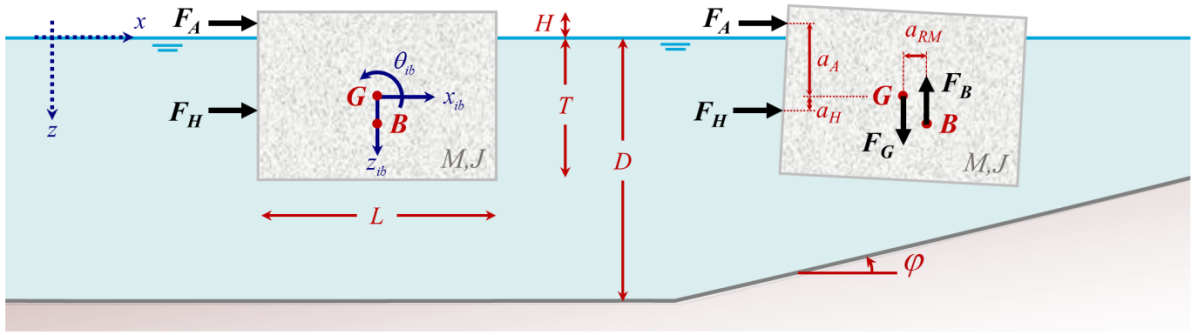

Figure 3. The degrees of freedom of and the forces on a free-floating iceberg.

Thus, the system of equations of motion for the free-floating iceberg reads:

$$\begin{aligned}
&\left(1+A_{xx}\right)Mx_{ib}-F_A-F_H=0\\
&\left(1+A_{zz}\right)Mz_{ib}+B_{zz}z_{ib}-F_G+F_B=0\\
&\left(1+A_{\theta\theta}\right)J\theta_{ib}+B_{\theta\theta}\theta_{ib}+F_Aa_A-F_Ha_H-F_Ba_{RM}=0
\end{aligned} \tag{1}$$

Here, F_A and F_H are respectively the resultant aero- and hydrodynamic drag forces working on the iceberg, while a_A and a_H are the arms of the corresponding forces with respect to the centre of gravity G of the iceberg. As the iceberg is simplified as an elliptical cylinder and its orientation and dimensions in the two-dimensional plane are assumed to be stable, i.e. it does not roll or yaw, its width W is constant over the height. Consequently, the aero- and hydrodynamic forces working on the iceberg are respectively obtained as:

$$F_A=\tfrac{1}{2}\rho_aC_aW\int_{-H}^{0}\left(u_a(z)-x_{ib}\right)\left|u_a(z)-x_{ib}\right|dz \tag{2}$$

$$F_H=\tfrac{1}{2}\rho_wC_wW\int_{0}^{T}\left(u_w(z)-x_{ib}\right)\left|u_w(z)-x_{ib}\right|dz \tag{3}$$

Here, ρ_a, ρ_w, C_a and C_w are respectively the air density, the water density and the air and water drag coefficients. Furthermore, $u_a(z)$ and $u_w(z)$ are respectively the wind (air) and current (water) profiles that are applied over the projected heights H and T of respectively the sail and the keel of the iceberg. The wind and current profiles are described as a function of the z-coordinate as:

$$u_a(z)=u_a^{10}\left(\frac{-z}{10}\right)^{\frac{1}{7}};\qquad u_w(z)=u_w^{\max}\left(\frac{z}{D}\right)^{\frac{1}{7}}. \tag{4}$$

Furthermore in Eq. (1), F_G and F_B respectively denote the weight and the buoyancy of the

iceberg, and a_{RM} is the stability lever arm, i.e. the arm between the centre of gravity and the centre of buoyancy due to pitch. The weight of the iceberg is assumed constant throughout and is straightforwardly obtained from the volume of its assumed shape and its density. The submerged volume, and thus the buoyancy of the iceberg, follows from the position of the iceberg in the water and thus depends on the heave and pitch motions of the iceberg. As stated previously, in this model only the viscous damping is accounted for, which in surge direction is already included in the aero- and hydrodynamic drag forces. The hydrodynamic viscous damping coefficients in respectively heave and pitch direction, denoted in Eq. (1) as B_{zz} and $B_{\theta\theta}$, are expressed in terms of the corresponding damping ratios as:

$$B_{zz} = 2\zeta_z\left(1+A_{zz}\right)M\omega_z; \qquad B_{\theta\theta} = 2\zeta_\theta\left(1+A_{\theta\theta}\right)J\omega_\theta. \tag{5}$$

For this model, the heave and pitch damping ratios are respectively chosen as $\zeta_z = 0,04$ and $\zeta_\theta = 0,02$ based on experimental values from free motion decay tests on a cylindrical object in water (Sudhakar and Nallayarasu, 2011). Furthermore, ω_z and ω_θ are the damped natural heave and pitch frequencies that follow from the uncoupled equations of motions for heave and pitch, thus found as:

$$\omega_z = \sqrt{\frac{\rho_w g A_{wl}}{\left(1+A_{zz}\right)M}}\sqrt{1-\zeta_z^2}; \qquad \omega_\theta = \sqrt{\frac{\rho_w g \nabla GM_L}{\left(1+A_{\theta\theta}\right)J}}\sqrt{1-\zeta_\theta^2}. \tag{6}$$

Added Mass of a Free-Floating Iceberg in Variable Water Depth

The hydrodynamic added mass coefficients, respectively denoted in Eq.s (1), (5) and (6) as A_{xx}, A_{zz} and $A_{\theta\theta}$ for respectively surge, heave and pitch, are derived from literature (Bai, 1976, Bass and Sen, 1985). In these contributions, the hydrodynamic coefficients are obtained using the potential flow theory by assuming that the flow is inviscid, irrotational and incompressible. The value of the hydrodynamic added mass coefficients for surge and heave depend on the distance between the bottom of the iceberg and the seabed, or more specifically, on the ratio between the water depth D and the height of the iceberg keel T. Figure 4 depicts the dependency of the added mass coefficients respectively in surge and heave directions as a function of the ratio D/T. The influence of the ratio D/T on the added mass coefficient for pitch however is negligible and therefore assumed constant.

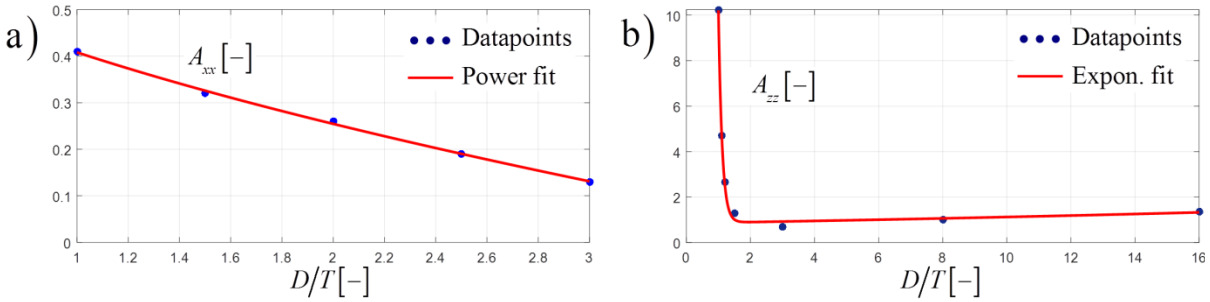

Figure 4. Dependency of the added mass coefficients on the iceberg-seabed distance.

In Figure 4, the added mass coefficients obtained by Bass and Sen (1985) and Bai (1976) for different values of the ratio D/T are given by blue dots, while the continuous red line gives a power fit for surge and an exponential fit for heave. For surge, the influence of the added mass coefficient on the ratio D/T appears to be relatively small. For heave however, the influence of the ratio D/T is significant. In fact, according to Bai (1976), the added mass of the iceberg in heave direction becomes infinitely large as the bottom of the iceberg touches the

seabed. In Figure 4b, the data-points have been fitted using a 3rd order polynomial resulting in an added mass coefficient for heave that is 10 times as large as the actual mass of the iceberg. For example, assuming that the free-floating iceberg is in a constant water depth of 150 m, i.e. $D/T = 1,5$, the added mass coefficients for surge, heave and pitch are constant and respectively found as $A_{xx} = 0,32$, $A_{zz} = 0,88$ and $A_{\theta\theta} = 0,04$.

Response of the Free-Floating Iceberg

The response of the free-floating iceberg subjected to winds and currents is obtained in the time domain by solving the system of ordinary differential Eq.s (1) using a Runge-Kutta scheme. To verify the modelling of the free-floating iceberg, the initial conditions for the iceberg are deliberately chosen far from its equilibrium condition. In this case, the initial position of the iceberg is arbitrarily chosen such that its top surface equals the waterline. For the wind and current velocities common average values are chosen as 30 km/h and 1,5 m/s respectively. As depicted by Figure 5 for two different icebergs, upon release from its initial position, the iceberg will ultimately attain a certain steady-state condition that is independent of the starting position, moving at a constant velocity. The iceberg reaches this constant velocity after nearly six hours covering a distance of about 30 km. Additionally, due to its initial vertical position and its own buoyancy, the iceberg oscillates for about 12 minutes before reaching a constant draft. Apparently, the rotation of the iceberg due to the applied constant wind and current is negligible. Note here that during the steady-state orientation, the icebergs restoring moment due to its pitch is equal to the moment caused by winds and currents.

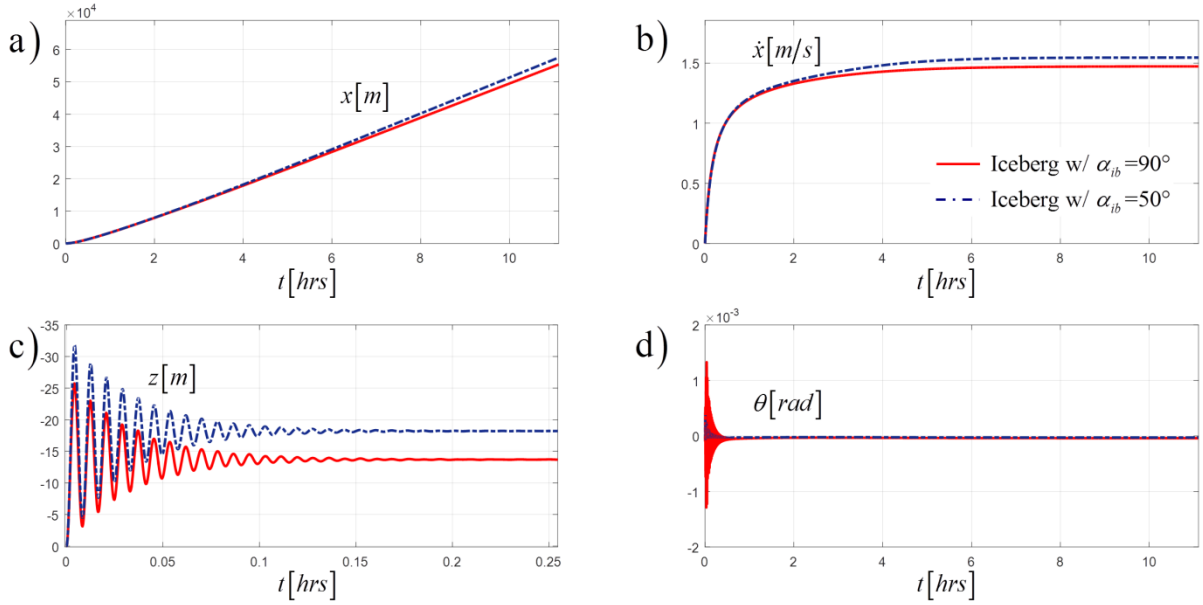

Figure 5. Response of the free-floating iceberg: a) surge; b) surge velocity; c) heave; d) pitch.

THE GROUNDING ICEBERG AND SEABED GOUGING

When an iceberg hits a seabed, the iceberg will penetrate that seabed as depicted in Figure 6b. Because of its inertia, the iceberg continues to move, leaving a seabed gouge in his wake, until the total kinetic energy of the iceberg has been dissipated by the iceberg-seabed interaction. The length and depth of these gouges depend on the mass, the shape and the drift velocity of

the iceberg, but also on the bathymetry of the seabed and the mechanical behaviour of the seabed soil (Green et al., 1983). Nevertheless, for a free-floating iceberg to cause seabed gouging, the seabed must at least have a slope somewhere. Although different configurations can be chosen, in this paper, the interaction of an iceberg with a continuous and constant sloping seabed is considered. Before considering the iceberg-seabed interaction in two-dimensional space using plane-strain conditions for the soil, first the interaction of the iceberg with a rigid seabed is addressed as a benchmark for the iceberg-soil interaction problem.

The Interaction of a Grounding Iceberg with a Rigid Seabed

To model the interaction with the rigid seabed, the first contact between iceberg and seabed is assumed to always occur at the corner C of the iceberg as depicted in Figure 6a. The normal and tangential forces that keep the iceberg from penetrating the rigid seabed are denoted as F_N and F_T respectively. Adding the normal and tangential forces to the system of equations of motion (1), previously obtained for the free-floating iceberg, yields the system of equations for the iceberg-rigid-seabed-interaction as:

$$\begin{aligned}
&\left(1+A_{xx}\right)Mx_{ib} - F_A - F_H + F_N \sin\varphi + F_T \cos\varphi = 0 \\
&\left(1+A_{zz}\right)Mz_{ib} + B_{zz}z_{ib} - F_G + F_B + F_N \cos\varphi - F_T \sin\varphi = 0 \\
&\left(1+A_{\theta\theta}\right)J\theta_{ib} + B_{\theta\theta}\theta_{ib} + F_A a_A - F_H a_H - F_B a_{RM} - r_N F_N + r_T F_T = 0
\end{aligned} \tag{7}$$

Here, r_N and r_T are the arms of respectively the normal and tangential forces with respect to the centre of gravity of the iceberg. The relation between the normal force F_N and the tangential force F_T is given the Coulomb friction coefficient μ, so that $F_T = \mu F_N$. Consequently, the given system of equations of motion consists of four unknowns, being the degrees of freedom of the iceberg and the normal force F_N and thus, to solve the above system of equations of motion, an additional equation is required. This equation follows from the change of the iceberg momentum due to interaction with the rigid seabed at point C. Accounting for the contributions due to the change both in linear momentum, i.e. the impulse, and in angular momentum, sometimes referred to as the angular impulse, over time, the velocity change of point C in the direction normal to the seabed slope over time is obtained as:

$$\frac{dv_N}{dt} = \frac{dv_N^{lin}}{dt} + \frac{dv_N^{ang}}{dt} = \left(\frac{1}{M} + \frac{r_N^2}{J}\right)F_N - \frac{r_N r_T}{J}F_T \tag{8}$$

Here, v_N denotes the velocity of the iceberg in the direction normal to the seabed slope. Accounting for the friction relation, then yields Eq. (8) as:

$$\left\{\frac{1}{M} + \frac{r_N}{J}\left(r_N - r_T\mu\right)\right\}F_N - \frac{dv_N}{dt} = 0 \tag{9}$$

For the remainder of the iceberg-rigid-seabed-interaction, it is assumed that the corner C remains on the seabed slope. Therefore, after the initial interaction of the iceberg with the rigid seabed, the velocity v_N in the direction normal to the seabed slope, as well as its time derivative, are equal to zero. However, right before the iceberg hits the seabed, the velocity of point C normal to the seabed slope is not equal to zero. In fact, right before the first iceberg-seabed interaction, the normal velocity v_N is known from the system of equations for the free-floating iceberg and the normal force F_N can thus be obtained by solving Eq. (9) numerically.

When the iceberg moves further along the seabed slope and the corner D also hits the seabed,

the bottom of the iceberg comes in full contact with the rigid seabed until the iceberg stops moving completely. In this case, the point of application of the normal and tangential forces is shifted to the centre-line of the iceberg. Note here that the above system of equations is only valid as long as the normal force F_N yields soil compression. Furthermore, note that when the iceberg hits the seabed, the iceberg keel is equal to the water depth and the ratio D/T is thus equal to 1. The corresponding added mass coefficients in Eq. (7) for surge, heave and pitch are respectively found as $A_{xx} = 0,41$, $A_{zz} = 10$ and $A_{\theta\theta} = 0,04$.

Iceberg-Soil Interaction for an Iceberg Penetrating the Seabed

When the iceberg interacts with a non-rigid seabed the corner C of the iceberg will penetrate the seabed as depicted in Figure 6b. The soil is assumed to behave as a cohesionless frictional material responding to external loads under fully drained conditions, i.e. with no generation of excess pore pressures (this assumption can be adopted for highly permeable sandy soils). During seabed gouging, the resistance of the soil to the iceberg motion is partly due to the deformation of the soil in front of the iceberg, as well as due to the frictional resistance at the bottom of the iceberg. The soil reaction in front of the iceberg is determined as a quasi-static passive force according to the plasticity approach by Hettiaratchi and Reece (1974). The normal and tangential resistance at the bottom of the iceberg are determined by a traditional bearing capacity equation for shallow foundations under inclined loads (Salgado, 2008).

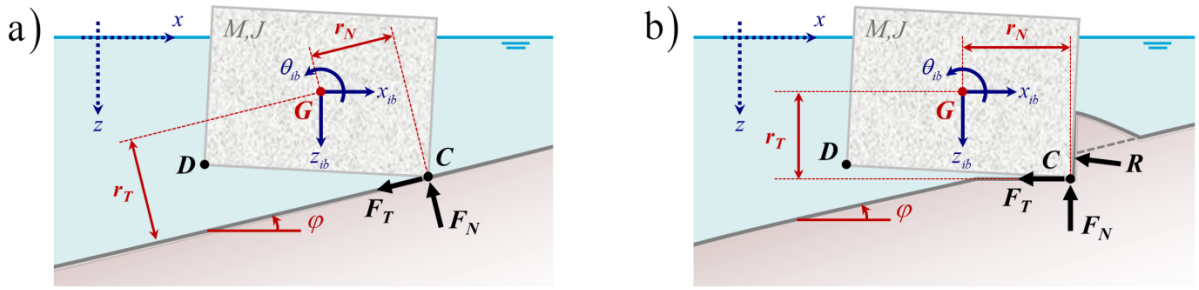

Figure 6. a) The iceberg hitting a rigid seabed; b) The iceberg penetrating the real-life seabed.

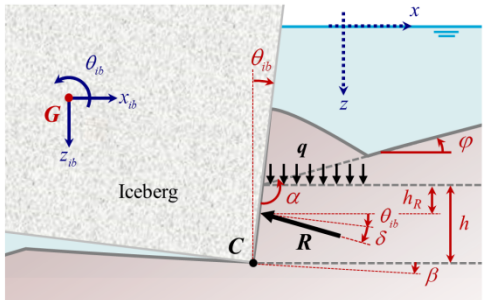

Figure 7. The resultant passive soil resistance force.

The resultant passive soil resistance force R is depicted in Figure 7. According to Hettiaratchi and Reece (1974), the resultant passive soil resistance force for a cohesionless soil reads:

$$R = R_1 + R_2 = qK_q h + \bar{K}_\gamma \gamma' h^2 \tag{10}$$

Here, q is the surcharge on the seabed surface, i.e. the amount of soil that is removed by the gouging of the iceberg and accumulates at the front and side of the iceberg, thereby yielding additional soil resistance, and γ' is the effective unit weight of the soil, while K_q and K_γ are the corresponding dimensionless soil resistance coefficients taken from the charts by

Hettiaratchi and Reece (1974). Additionally, h is the vertical distance between the corner C of the iceberg and the seabed slope. Following Hettiaratchi and Reece (1975), the angle δ of the resistance force R for cohesionless soils follows from the angle of internal friction of the soil ϕ and the difference between the rake angle α and the angle β that describes the direction of forward motion of the iceberg-seabed interface with respect to the horizontal, so that:

$$\tan\delta = \frac{\sin\phi \cdot \sin\left(270 - \phi - 2\left(\alpha - \beta\right)\right)}{1 + \sin\phi \cdot \cos\left(270 - \phi - 2\left(\alpha - \beta\right)\right)} \tag{11}$$

The point of application of the force R cannot be determined exactly because the actual distribution of soil stresses along the iceberg edge is unknown. According to Hettiaratchi and Reece (1974), the vertical distance between the seabed surface and the point of application of the force R, denoted as h_R, can be approximated as:

$$h_R = h\left(\frac{3R_1 + 4R_2}{6R}\right) \tag{12}$$

As the gouging depth of an iceberg is generally smaller than its width, the ultimate bearing capacity of the iceberg during seabed gouging is determined using Terzaghi's bearing capacity equation for shallow foundations in combination with the capacity correction factors by Brinch Hansen (1970). Accordingly, the maximum vertical pressure that the soil is able to provide at the bottom of the iceberg is determined as:

$$q_{ult} = 0,3 s_\gamma d_\gamma i_\gamma b_\gamma g_\gamma \gamma' B N_\gamma \tag{13}$$

Here, a factor 0,3 is used to account for the elliptical shape of the iceberg bottom instead of a factor 0,5 that is used for a strip footing. Furthermore, s_γ and d_γ are respectively shape and depth factors, while i_γ, b_γ and g_γ are load inclination, base inclination and ground inclination factors respectively. The expressions and values for these factors are taken from Salgado (2008). As before, γ' is the effective unit weight of the soil, while N_γ is the corresponding bearing capacity factor and B equals the contact length between the iceberg and the soil during gouging, which varies over time. The normal force F_N is then found at each time step as $F_N = q_{ult} A_c$, where A_c yields the soil-iceberg contact area during seabed gouging. Here, both the normal force F_N and the tangential force F_T are assumed to act in the middle of the contact length. To determine the ratio between the normal and the tangential force, the load inclination factor must be known and vice versa. Since both the ratio and the load inclination factor are unknown prior to each time step, the load inclination factor is found iteratively. Initially, the load inclination factor i_γ is set equal to 1, i.e. a vertical load reaction, or when available, equal to the final load inclination factor from the previous time step. Then, the corresponding motions of the iceberg are determined numerically and the normal and tangential forces are back-calculated from the system of equations of motion. The ratio between the normal and tangential force yields a new load inclination factor as input for the same time step. The iteration is repeated until the load inclination factor i_γ converges to a given threshold. The ratio between F_T and F_N has a lower bound given by the soil-iceberg interface friction angle, relevant to the limit case of horizontal sliding of the bottom iceberg surface.

Accounting for both the resistance of the soil in front and at the bottom of the iceberg, the system of equations of motion for the iceberg follows as:

$$\begin{aligned}
&\left(1+A_{xx}\right)Mx_{ib}-F_A-F_H+F_T\cos\beta+F_N\sin\beta+R_x=0\\
&\left(1+A_{zz}\right)Mz_{ib}+B_{zz}z_{ib}-F_G+F_B-F_T\sin\beta+F_N\cos\beta+R_z=0\\
&\left(1+A_{\theta\theta}\right)J\theta_{ib}+B_{\theta\theta}\theta_{ib}+F_Aa_A-F_Ha_H-F_Ba_{RM}+r_TF_T-r_NF_N+r_{Rx}R_x-r_{Rz}R_z=0
\end{aligned} \tag{14}$$

Here, R_x and R_z are respectively the horizontal and vertical components of the resistance force R and are thus respectively obtained as $R_x=R\cos\left(\theta_{ib}+\delta_r\right)$ and $R_z=R\sin\left(\theta_{ib}+\delta_r\right)$. It should here be noted that in the model by Hettiaratchi and Reece, the seabed surface is assumed horizontal, while our seabed has a constant positive slope. The slope is accounted for by including the soil volume of the seabed slope in the surcharge. Additionally, Hettiaratchi and Reece assume that the soil-structure interface does not rotate, but translates at a sufficiently slow pace so that inertia loads are negligible. Here, the rotation of the iceberg is incorporated. The influence of the rotation on the passive soil resistance however is neglected by choosing the time step sufficiently small. In addition, this reduces the error by neglecting the influence of the inertia and allows for the quasi-static determination of the soil resistance.

The Iceberg Hitting a Rigid Seabed Versus the Iceberg Penetrating the Seabed

The interaction of an iceberg hitting the rigid seabed, as well as the process of seabed gouging of an iceberg has been simulated solving the corresponding systems of equations in the time domain. The resulting iceberg response is depicted in Figure 8, where the continuous red and dashed blue lines respectively give the interaction with the rigid and the real seabed.

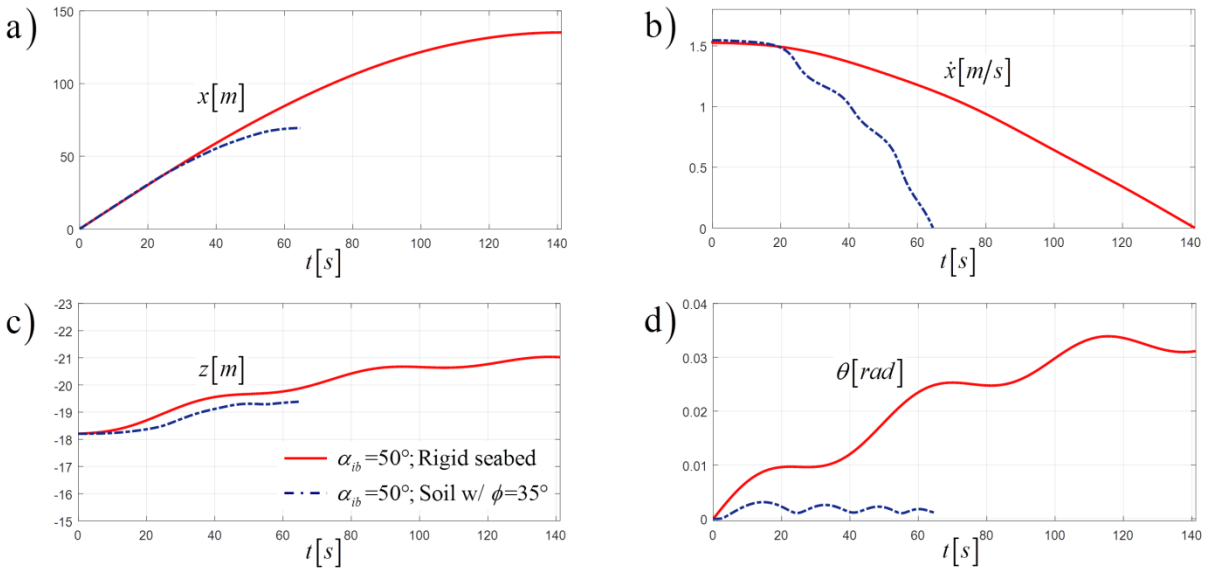

Figure 8. Iceberg interacting with the seabed: a) surge; b) surge velocity; c) heave; d) pitch.

For both considered cases, the initial conditions are assumed equal to the steady-state conditions obtained for the free-floating iceberg response. As the hydrodynamic parameters are chosen equal to those for the free-floating iceberg as well, the iceberg-seabed interaction may be considered to start at the end of the free-floating iceberg response. The iceberg-seabed interaction process consists of two distinct phases, being (i) the phase where the water depth decreases due to the seabed slope until the iceberg touches the seabed, and (ii) the phase of interaction between the iceberg and the seabed until the iceberg comes to a standstill. Evidently, the first phase is identical for the two cases, and the difference in Figure 8 only occurs after the iceberg hits the seabed.

Here, the seabed consists of sand with a density $\rho_s = 2080\,kg/m^3$ and has a constant slope of $\varphi = 2°$. The angle of internal friction of the soil is chosen as $\phi = 35°$ and the cohesion is assumed zero. Furthermore, the iceberg-seabed friction coefficient is chosen as $\mu = 0,39$.

Figure 8a and Figure 8b show that the distance travelled by the iceberg interacting with the rigid seabed is significantly larger than that of the iceberg gouging the seabed. As the iceberg cannot penetrate and therefore does not gouge the rigid seabed, the resistance of the rigid seabed against the iceberg motion exclusively consists of the Coulomb friction and thereby highly underestimates the seabed resistance. The distance travelled by the iceberg from the point of first contact with the seabed until it comes to a standstill should therefore be considered as an absolute upper limit for seabed gouging. Additionally, it can be seen from Figure 8c and Figure 8d that the iceberg interacting with the rigid seabed moves up the seabed slope, while it tilts backward until the iceberg rotation coincides with that of the rigid seabed. The iceberg gouging the seabed however, does not follow the sloping seabed at all. Due to the significantly higher seabed resistance forces, the iceberg tilts forward and digs itself into the soil, thereby further increasing the seabed soil resistance causing a fast deceleration of the iceberg.

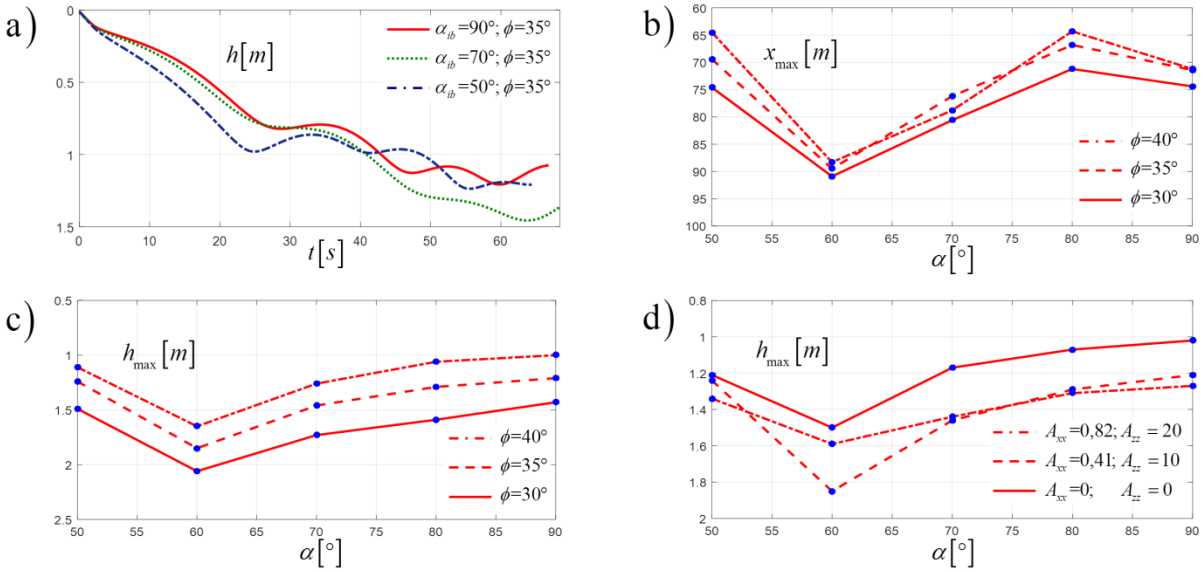

Figure 9. a) gouge depth for several icebergs; b) gouge length versus rake angle for several internal friction angles; c) maximum gouge depth versus rake angle for several internal friction angles; d) maximum gouge depth versus rake angle for varying added mass coefficients.

Figure 9a shows the gouge depth, or seabed penetration, as a function of time for three icebergs with different rake angles. These penetrations show an increasing trend due to the constant seabed slope. It is striking that the iceberg Bertha, with a rake angle $\alpha_{ib} = 50°$ nearly has the smallest maximum penetration and requires the shortest time to come to a standstill, which in fact does not necessarily mean that it has the shortest gouging length. This is verified by Figure 9b that shows the relation between the gouging length and the rake angle for three purely frictional sands with an internal friction angle $\phi = 30°$, $\phi = 35°$ and $\phi = 40°$ respectively. From Figure 9b, it appears that the influence of the rake angle on the gouging length is larger the influence of the soil strength. Figure 9c shows the maximum gouge depth, or maximum seabed penetration, as a function of the iceberg rake angle for the same three sands that have previously been considered in Figure 9b. In this case, the gouge depth is clearly larger for soils with smaller internal friction angle and vice versa. From Figure 9b and

Figure 9c it follows that the shortest gouges are also the deepest gouges and generally occur for icebergs with a rake angle of around 60°. Finally, Figure 9d again shows the maximum gouge as a function of the rake angle, but now for three different sets of added mass coefficients to determine the sensitivity of the iceberg-soil interaction on theses added mass coefficients. As a general case, the added mass coefficients are used that were previously determined for a *D/T*-ratio equal to 1. In addition, we have here considered added mass coefficients that are twice as large, as well as added mass coefficients that are equal to 0. It should be noted here that the added mass coefficients used in this paper are derived on measurements of the added mass of two-dimensional cylinders heaving in a finite water depth. For frustum-shaped icebergs with small rake angles, the added mass coefficients are therefore slightly overestimated. However, for frustum-shaped icebergs with large rake angles, this difference may be significant and the results may be unreliable.

DISCUSSION, CONCLUSIONS AND FURTHER WORK

This contribution present the results of the first stage of an attempt to dynamically correct model both the free-floating iceberg as well as the dynamic iceberg-soil interaction during seabed gouging. Clearly, as the resulting two-dimensional iceberg model is a work-in-progress, the model is still subject to significant improvements.

First of all, the currently assumed shape of iceberg Bertha is far from realistic. To incorporate the variation of the geometry of the iceberg, and thus to consider more realistic iceberg shapes, the iceberg is considered to be comprised of a set of horizontal layers, where the width, length and side angle may be chosen independently for each layer. This yields a variation of the hydrodynamics over the height of the iceberg, as well as the ability to change the angle of the iceberg-soil interface. Furthermore, to more correctly describe the iceberg-soil interaction during seabed gouging, it is envisaged to introduce a failure criterion that describes the failure of the iceberg keel, thereby allowing the iceberg geometry to change due to its interaction with the soil. Although posing considerable modelling challenges, this will additionally allow us to account for the stability of the iceberg during seabed gouging.

REFERENCES

BAI, K. J. 1976. The added mass of two-dimensional cylinders heaving in water of finite depth. *Journal of Fluid Mechanics,* 81**,** 21.

BARRETTE, P. D. 2011. Offshore pipeline protection against seabed gouging by ice: An overview. *Cold Regions Science and Technology 69***,** 3-20.

BASS, D. W. & SEN, D. 1985. Added mass and damping coefficient for certain 'realistic' iceberg models. *Cold Regions Science and Technology,* 12**,** 13.

BRINCH HANSEN, J. A. 1970. Revised and extended formula for bearing capacity. *Bulletin no. 28.* Copenhagen: Danish Geotechnical Institute Copenhagen.

DIEMAND, D. 2001. Icebergs. *Encyclopedia of Ocean Sciences***,** 1255-1264.

GREEN, H. P., REDDY, A. S. & CHARI, T. R. Iceberg scouring and pipeline burial depth. 7th International Conf. on Port and Ocean Engineering under Arctic Conditions (POAC), 1983 Helsinki, Finland. 280-288.

HETTIARATCHI, D. R. P. & REECE, A. R. 1974. The calculation of passive soil resistance.

Géotechnique, 24**,** 289-310.
HETTIARATCHI, D. R. P. & REECE, A. R. 1975. Boundary wedges in two-dimensional passive soil failure. *Géotechnique,* 25**,** 197-219.
HODGSON, G. J., LEVER, J. H., WOODWORTH-LYNAS, C. M. T. & LEWIS, C. F. M. 1988. Dynamics of Iceberg Grounding and Scouring. St. John's, Nfld.
KIOKA, S. & SAEKI, H. Mechanisms of Ice Gouging. 5th International Offshore and Polar Engineering Conf. , June 11-16 1995 The Hague, The Netherlands. 398-402.
SALGADO, R. 2008. *The Engineering of Foundations,* New York, McGraw-Hill.
SUDHAKAR, S. & NALLAYARASU, S. Influence of heave plate on hydrodynamic response of spar. 30th International Conf. on Ocean, Offshore and Arctic Engineering (OMAE), June 19-24 2011 Rotterdam, The Netherlands. 437-447.
YOON, K.-Y., CHOI, K. & PARK, H.-I. 1997. A Numerical Simulation to Determine Ice Scour and Pipeline Burial Depth. *International Offshore and Polar Engineering Conf.* Honolulu, USA.